OXFORD

Vascular injury is associated with repetitive head impacts and tau pathology in chronic traumatic encephalopathy

Daniel Kirsch [iD], BA,[1,2,3] Arsal Shah, BS,[1,2,4] Erin Dixon, BA,[1,2,4] Hunter Kelley, BA, MSc,[1,2]
Jonathan D. Cherry [iD], PhD,[1,2,3] Weiming Xia, PhD,[1,4] Sarah Daley, BS,[1,4]
Nurgul Aytan, PhD,[1,2] Kerry Cormier, BA,[1,4] Carol Kubilus, RT,[1,4] Rebecca Mathias, HT,[1,2]
Victor E. Alvarez, MD,[1,2,4,5] Bertrand R. Huber, MD, PhD,[1,2,3,4,5] Ann C. McKee, MD,[1,2,3,4,5]
Thor D. Stein [iD], MD, PhD[1,2,3,4]*

[1]Boston University Alzheimer's Disease and CTE Center, Boston University School of Medicine, Boston, Massachusetts, USA
[2]VA Boston Healthcare System, Boston, Massachusetts, USA
[3]Department of Pathology and Laboratory Medicine, Boston University School of Medicine, Boston, Massachusetts, USA
[4]VA Bedford Healthcare System, Bedford, Massachusetts, USA
[5]Department of Neurology, Boston University School of Medicine, Boston, Massachusetts, USA

*Send correspondence to: Thor D. Stein, MD, PhD, Boston University Alzheimer's Disease and CTE Center, Boston University School of Medicine, 72 E Concord Street, B7800, Boston, MA 02118, USA; E-mail: tdstein@bu.edu

ABSTRACT

Chronic traumatic encephalopathy (CTE) is a neurodegenerative disease linked to repetitive head impacts (RHI) and characterized by perivascular hyperphosphorylated tau (p-tau) deposits. The role of vascular injury, blood-brain barrier leakage, and neuroinflammation in CTE pathogenesis is not well understood. We performed quantitative immunoassays for intercellular adhesion molecule 1 (ICAM1), vascular cellular adhesion molecule 1 (VCAM1), and C-reactive protein (CRP) within the postmortem dorsolateral frontal cortex of participants with and without a history of RHI and CTE (n = 156), and tested for associations with RHI, microgliosis, and tau pathology measures. Levels of vascular injury-associated markers ICAM1, VCAM1, and CRP were increased in CTE compared to RHI-exposed and -naïve controls. ICAM1 and CRP increased with RHI exposure duration ($p < 0.01$) and were associated with increased microglial density ($p < 0.001$) and tau pathology (AT8, p-tau396, p-tau202; $p < 0.05$). Histologically, there was significantly increased ICAM1 staining of the microvasculature, extracellular space, and astrocytes at the sulcal depths in high stage CTE compared to both low stage CTE and controls. Multifocal perivascular immunoreactivity for serum albumin was present in all RHI-exposed individuals. These findings demonstrate that vascular injury markers are associated with RHI exposure, duration, and microgliosis, are elevated in CTE, and increase with disease severity.

KEYWORDS: Chronic traumatic encephalopathy (CTE), Inflammation, Neurodegeneration, p-tau, RHI, Vascular injury

INTRODUCTION

Chronic traumatic encephalopathy (CTE) is a neurodegenerative disorder associated with exposure to repetitive head impacts (RHI) and characterized by the deposition of hyperphosphorylated tau protein (p-tau) as neurofibrillary and astrocytic tangles, which are distributed around blood vessels and at the depths of the cortical sulci (1–4). It is estimated that over 200 million individuals in the United States have been exposed to RHI through contact sports, military activities, and interpersonal violence (5). Multiple studies have demonstrated a direct relationship between the severity of p-tau pathology in CTE and the dose and duration of RHI exposure (2, 6–8). Quantification of tau phosphorylation sites including Thr181 (p-tau181), Ser202 (p-tau202), Thr231 (p-tau231), and Ser396 (p-tau396) has shown that levels of

p-tau202, p-tau231, and p-tau396 are increased and p-tau181 decreased in the frontal cortex in CTE, and that p-tau202 levels are associated with RHI exposure duration (9).

Although the number of years of contact sport play has been associated with increased risk for CTE and more severe CTE stage, the absolute risk for developing CTE following a period of RHI is unknown (6). Mez et al (6) reported that in a postmortem cohort of 266 American football players, the odds of CTE doubled for every 2.6 years of football played. Microvascular injury, endothelial damage, blood-brain barrier (BBB) disruption and increased permeability, and neuroinflammation are possible acute consequences of RHI that may, if persistent, drive CTE pathogenesis and progression (10–13). Doherty et al (14) reported that in a case of CTE, there was markedly diminished immunoreactivity of BBB-associated

tight junction proteins in regions of p-tau pathology, suggesting a role of BBB disruption in this disease. The perivascular location of the initial p-tau aggregates in CTE, around small blood vessels at cortical depths, is consistent with areas of the brain subject to the greatest biomechanical tissue strain during head impacts (15–18). This may be partially explained mechanically by the heterogenous composition of the brain and its surroundings, with differences in the physical and mechanical properties between the vasculature, which is relatively elastic, and the brain parenchyma, which is comparatively stiff (15, 16). The distribution of impact forces at the interface between the vasculature and brain parenchyma may result in shear stress that disrupts the endothelium and initiates an inflammatory response (16, 19–21). Leakage of serum proteins from damaged microvasculature activates microglia and induces an inflammatory astrocytic phenotype, which may exacerbate neuroinflammation after RHI and in CTE (22–25). It has been previously reported that leakage of fibrinogen and immunoglobulin G is found histologically even years after a single traumatic brain injury (TBI) (26). Repetitive microvascular injury and sustained neuroinflammation secondary to RHI exposure is a potential mechanism underlying CTE pathogenesis and progression (10, 11).

Several proteins have been associated with both acute and chronic neurovascular injury, including intercellular adhesion molecule 1 (ICAM1), vascular cell adhesion molecule 1 (VCAM1), and C-reactive protein (CRP) (27–29). ICAM1, also known as CD54, and VCAM1, also known as CD106, are cell surface glycoprotein molecules expressed primarily on vascular endothelial cells. These members of the immunoglobulin superfamily function to bind to transmembrane integrins, such as the lymphocyte function-associated antigen 1 (LFA1) or macrophage-1 receptor (MAC1), on circulating leukocytes and tissue microglia, promoting extravasation into the parenchyma (30–33). The relationship between traumatic brain injury and ICAM1 cerebrospinal fluid and serum levels has been established by many groups, demonstrating that ICAM1 levels increase with injury severity (28, 34–37). ICAM1 has also been observed to be expressed in a subset of reactive astrocytes in cases of Alzheimer disease (AD), possibly contributing to the formation of senile amyloid-ß plaques and p-tau tangles (38). CRP is an acute phase reactant elaborated in response to inflammatory stimuli, and is produced by neurons and endothelial cells in the setting of injury and neurodegeneration (29, 39, 40). CRP has been shown to increase endothelial activation and expression of ICAM1 and VCAM1 by endothelial cells (40–42).

Although the role of acute vascular damage following TBI is well established, the roles of chronic neurovascular-mediated inflammation and vascular damage following mild head impacts over a prolonged period of time and in CTE pathogenesis are largely unknown. We hypothesized that levels of vascular injury-associated markers are increased in RHI-exposed individuals and that levels increase with duration of RHI exposure and with the development of CTE. We further tested the association of levels of vascular injury associated proteins with measures of p-tau pathology in CTE, utilizing biochemical and histological methods. Finally, we examined the spatial distribution of markers of vascular injury in CTE and the degree of colocalization with endothelial cells, glia, and p-tau pathology.

MATERIALS AND METHODS

All experimental groups and abbreviations are listed and defined in Supplementary Data Table S1.

Ethics approval statement

IRB approval for the brain donation program was obtained through the VA Boston and Bedford Healthcare Systems and Boston University School of Medicine.

Participants
Immunoassay group

A total of 156 autopsy participants were included in this study. At the time of study initiation, there were 417 male autopsy participants in the Understanding Neurological Injury and Traumatic Encephalopathy Brain Bank (UNITE) with frozen tissue available and complete neuropathological diagnostic reports. Three hundred nine individuals were excluded from this study due to neuropathological diagnosis of vascular disease, AD, neocortical Lewy body disease, motor neuron disease (MND), and/or frontotemporal lobar degeneration-tau (FTLD-tau). A diagnosis of AD was determined using the National Institute of Aging Reagan criteria and included intermediate and high probability of dementia caused by AD (43, 44). The remaining participants with a history of RHI exposure, primarily through participation in contact sports, were selected for study (n = 108). RHI exposure was determined based on retrospective clinical questionnaires with family and verified with public record databases if the individual played at the professional level. In addition, participants without a history of RHI exposure were selected from the Framingham Heart Study Brain Bank (FHS) and the Veterans Affairs National Posttraumatic Stress Disorder Brain Bank (NPBB) using the same neuropathological exclusion criteria (n = 48). Acute TBI, defined as the presence of hemorrhage, contusion, or other evidence of acute trauma to brain and/or dura upon examination by the neuropathologist, did not exclude participation in this study, though was noted if present (n = 12). None of the included cases were diagnosed with meningitis or encephalitis at autopsy (Table 1). Subjects were categorized based on their RHI exposure history and CTE diagnosis into 4 groups: "No RHI No CTE" (n = 39), "RHI No CTE" (n = 36), "Low CTE" (Stages I and II; n = 31), and "High CTE" (Stages III and IV; n = 50) (2, 4). Consents for brain donation and research participation were provided by donor next of kin. Institutional review boards from Boston University School of Medicine and VA Bedford Healthcare System approved brain donation, postmortem clinical record review, neuropathological evaluation, and clinical interviews with donor family members.

Histology group

A smaller representative subset of individuals was formed from the immunoassay group for histological analysis of paraffin

Table 1. Demographic, exposure, and pathological measures between pathology groups

	No RHI No CTE	RHI No CTE	Low CTE	High CTE	
Sample size (n)	39	36	31	50	
Brain bank					p < 0.001
UNITE	0	27	31	50	
FHS	24	7	0	0	
NPBB	15	2	0	0	
Age at death (SEM)	71.21 (3.15)	52.64 (3.92)	52.77 (3.01)	73.38 (1.62)	p < 0.0001[a,d,e,f]
Postmortem interval (SEM)	21.03 (2.10)	46.61 (5.77)	48.28 (3.58)	43.86 (2.92)	p < 0.0001[a,b,c]
RHI n (% exposed)	0 (0%)	35 (100%)	31 (100%)	50 (100%)	
RHI exposure years (SEM)	0 (0)	9.06 (1.39)	16.65 (2.29)	17.02 (0.93)	p < 0.0001[a,b,c,e]
Types of RHI exposure					
Primary sport					p < 0.001[a,b,c]
Football	0	31	29	49	
Hockey	0	2	1	0	
Boxing	0	0	1	1	
Soccer	0	3	0	0	
Military/other exposure	0	4	3*	2	
CTE stage n (%)					p < 0.001
Stage I	0 (0%)	0 (0%)	14 (45.16%)	0 (0%)	
Stage II	0 (0%)	0 (0%)	17 (54.84%)	0 (0%)	
Stage III	0 (0%)	0 (0%)	0 (0%)	28 (56.00%)	
Stage IV	0 (0%)	0 (0%)	0 (0%)	22 (44.00%)	
Atherosclerosis[†] y/n (%)	8/15 (34.78%)	8/27 (22.86%)	3/28 (9.68%)	17/33 (34.00%)	p = 0.070
Arteriolosclerosis[†] y/n (%)	16/7 (69.57%)	13/22 (37.14%)	13/18 (41.94%)	33/17 (66.00%)	p = 0.012
Acute TBI[‡] n (%)	3 (15%)	4 (13.33%)	0 (0%)	5 (10%)	p = 0.230
APOE ε4 presence +/− (%)	5/18 (21.74%)	9/26 (25.71%)	14/17 (45.16%)	14/36 (28.00%)	p = 0.084

Data are presented as mean (SEM) years for age at death and contact sports exposure and as #yes (%) unless otherwise indicated.

CTE: chronic traumatic encephalopathy; RHI: repetitive head impacts; TBI: traumatic brain injury; Low CTE: Stages I–II; High CTE: Stages III–IV.

* One individual in this group reported RHI exposure due to occupation as a firefighter.

† Arteriolosclerosis and atherosclerosis were defined as moderate to severe disease.

‡ Acute TBI was defined as the presence of hemorrhage, contusion, or other evidence of acute trauma to brain and/or dura upon examination by neuropathologist.

p values determined using ANOVA or χ^2 test for proportions between all pathology groups. Significant (p < 0.05) post hoc comparisons are indicated as follows: a: No RHI No CTE vs RHI No CTE, b: No RHI No CTE vs Low CTE, c: No RHI No CTE vs High CTE, d: RHI No CTE vs Low CTE, e: RHI No CTE vs High CTE, f: Low CTE vs High CTE.

embedded DLF tissue. This subgroup was age, CTE stage, and RHI matched to the larger immunoassay group. Those who died by head trauma, hanging, or asphyxia, or noted to have acute head trauma postmortem were excluded from this group due to the possible confounding effects on ICAM1 and albumin staining. Based on the 28% difference in ICAM1 levels, we determined that histological groups of at least n = 10 would be powered to detect differences. Subjects were grouped based on their CTE diagnosis into 3 groups: No CTE (n = 10), Low CTE (Stage I, n = 12 and Stage II, n = 12), and High CTE (Stage III, n = 13 and Stage IV, n = 10; Table 2).

Tissue collection, specimen processing, and pathological assessment

Fresh tissue was obtained from the dorsolateral prefrontal cortex (Brodmann area 8/9) upon receipt of brain donation and the remaining tissue was fixed in periodate-lysine-paraformaldehyde (PLP) for at least 3 weeks. The DLF was selected as it is a common site of initial CTE p-tau pathology and often accumulates a relatively high p-tau burden in advanced disease compared to other areas (1, 2). Neuropathological assessment was then performed following procedures and criteria previously established for the UNITE, FHS, and NPBB studies (45–47).

APOE genotyping

APOE genotype was determined from DNA extracted from participant brain tissue using single nucleotide polymorphism (National Center for Biotechnology Information SNPs rs429358 and rs7412) as previously described (48, 49). Participants were divided into *APOE* ε4 positive, which included genotypes ε2/ε4 (n = 3), ε3/ε4 (n = 37), and ε4/ε4 (n = 2), and *APOE* negative, including ε2/ε2 (n = 2), ε2/ε3 (n = 12), and ε3/ε3 (n = 83).

Vascular injury marker immunoassay

ICAM1, VCAM1, and CRP were detected and measured in fresh tissue lysate from the DLF using the Mesoscale Discovery V-PLEX Plus Neuroinflammation Panel Kit (Mesoscale Discovery [MSD], Rockville, MD). Grey matter was isolated from frozen brain tissue on dry ice and weighed. Ice-cold RIPA buffer (#89901, Thermo Scientific, Waltham, MA) was added to the grey matter at 5 mL RIPA: 1 g brain wet weight and homogenized with Qiagen Tissue Lyser LT at 50 Hz for 5 minutes (Qiagen, Germany). The homogenate was centrifuged at 17,000g at 4°C for 15 minutes, then the supernatant was aliquoted and stored at −80°C until use for vascular injury immunoassay panel (MSD, K15198G), which was performed according to the manufactory instructions. Wash buffer was prepared by combining 15 mL of MSD 20× wash buffer with

Table 2. Histology cohort demographics

	No CTE	**Mild CTE**	**Severe CTE**	**p value**
Sample size (n)	10	24	23	
Cohort				
UNITE	10 (100%)	24 (100%)	23 (100%)	
CTE stage				p < 0.001
McKee Stage I	0	12	0	
McKee Stage II	0	12	0	
McKee Stage III	0	0	13	
McKee Stage IV	0	0	10	
Age at death (SEM)	60.11 (2.63)	64.30 (2.39)	69.76 (2.24)	p = 0.521
Sex male (%)	10 (100%)	24 (100%)	23 (100%)	
RHI y/n (% exposed)	10 (100%)	24 (100%)	23 (100%)	
Exposure years (SEM)	8.67 (2.08)	15.80 (2.43)	16.70 (1.57)*	p > 0.05[a,c], p = 0.030[b]

Data are presented as mean (SEM) years for age at death and as # yes/# no (%) unless otherwise indicated.
CTE: chronic traumatic encephalopathy; RHI: repetitive head impacts.
  * Data for one individual in this group not available. p Values determined using ANOVA or χ^2 test for proportions between groups.
Significant (p < 0.05) post hoc comparisons are indicated as follows: a: No CTE vs Low CTE, b: No CTE vs High CTE, c: Low CTE vs High CTE.

285 mL of deionized water. The immunoassay plates were washed with wash buffer 3 times before 50 μL of diluted (1:5) tissue lysate was added after which the plates were sealed and incubated for 2 hours with agitation at room temperature. 1× detection antibody solution was prepared from stock solutions by combining 60 μL of 50× SULFO-TAG anti-human CRP antibody, 60 μL of 50× SULFO-TAG anti-human VCAM1 antibody, and 60 μL of 50× SULFO-TAG anti-human ICAM1 antibody with 2,760 μL of Diluent 101. The plates were then washed 3 times with wash buffer before 25 μL of 1× detection antibody solution was pipetted into each well, and the plates were sealed and incubated for 1 hour with agitation at room temperature. The plates were washed 3 times with wash buffer, and then 150 μL of read buffer T was added to each well. Immunoassay plates were read using the SECTOR Imager 2400 to quantitate protein levels, which were expressed as pg/mL (MSD).

Phospho-tau immunoassay measurement

Freshly prepared, ice cold 5M Guanidine Hydrochloride in Tris-buffered saline (20 mM Tris-HCl, 150 mM NaCl, pH 7.4) containing 1:100 Halt protease inhibitor cocktail (Thermo Fischer Scientific) and 1:100 Phosphatase inhibitor cocktail 2 & 3 (Sigma-Aldrich, St. Louis, MO) was added to the brain tissue at 5:1 (5M guanidine hydrochloride volume [mL]: brain wet weight [g]) and homogenized with Qiagen Tissue Lyser LT at 50 Hz for 5 minutes. The homogenate was then mixed (regular rocker) overnight at room temperature. The lysate was diluted with 1% Blocker A (MSD #R93BA-4) in wash buffer at 1:300 for p-tau181 (MSD #K250QND), p-tau202 (MSD N45CB-1), and p-tau231 (MSD #K15121D-2). The lysate was diluted with 1% Blocker A (Meso Scale Discovery [MSD], #R93BA-4) in wash buffer at 1:4000 for $A\beta_{1-38}$, $A\beta_{1-40}$, and $A\beta_{1-42}$ (MSD #K15200E-2). Samples were subsequently centrifuged at 17,000g and 4°C for 15 minutes after which the supernatant was applied to the immunoassays. To capture tau phosphorylated at Thr residue 181, antibody AT270 was used and the detecting antibody was the biotinylated HT7 that recognizes residue 159–163 of tau (Thermo Scientific). To measure levels of p-tau396, brain lysate as prepared above was diluted 1:300 by 1% Blocker A (MSD #R93BA-4) in wash buffer. Rabbit monoclonal antibody against p-tau 396 (Abcam, ab156623) was used as the capturing antibody and biotinylated HT-7 was used as a detecting antibody in a standard sandwich ELISA. SULFO-TAG conjugated streptavidin secondary antibody was used for signal detection by the MSD platform. Internal calibrators of p-tau and tau were commercially available (MSD) (50). Standards with known concentrations were used for Aβ (MSD) as previously described (9). All standards and samples were run in duplicate. Measurements were performed using the SECTOR Imager 2400 (MSD). Levels of p-tau181 were expressed as units/mL, and levels of p-tau202, p-tau231, and p-tau396 were expressed as μg/g.

Immunohistochemistry staining
Immunofluorescence staining

Slides were cut from paraffin embedded dorsolateral frontal cortex tissue at a thickness of 10 μm. Sections to be stained for ICAM1 and albumin via IF or IHC were stained as soon as possible after being cut (no more than a month prior) due to epitope oxidation. Slides were deparaffinized in a series of xylene, 100% ethanol, 95% ethanol, and 70% ethanol baths. A 30-minute endogenous peroxidase block with methanol peroxide was performed between the 95% and 70% ethanol baths. Heat induced epitope retrieval was performed for each antigen with a BioWave microwave (BioWave Corporation, Norwalk, CT) according to Supplementary Data Table S2. All incubations were performed at room temperature. All antibodies were diluted in a solution of 1% donkey serum in 0.1% Triton-X 100 phosphate buffered saline (PBS). Before each primary antibody, nonspecific binding was blocked by using 3% donkey serum in 0.1% Triton-X 100 PBS. Primary antibody incubation was performed for 1 hour, with specific dilutions for each antibody listed in Supplementary Data Table S2. Diluted secondary antibodies were incubated after washing slides with tris-buffered-saline-tween-20 (TBST) buffer. Akoya Opal dyes 480, 520, 570, and 620 (Akoya Biosciences, Inc., Marlborough, MA) were diluted in Akoya Color Amplification Diluent at 1:150 and applied for 10 minutes. If another antibody was to be applied, the slides were placed the appropriate solution for

antigen retrieval and the previous steps were repeated. After all markers had been applied, DAPI solution (Akoya Biosciences, Marlborough, MA) (2 drops DAPI: 1 mL TBST) was applied to the slides for 5 minutes before slides were washed in TBST and coverslipped with ProLong Diamond Antifade Mounting Media (Invitrogen, Carlsbad, CA) and sealed with clear nail polish (Sally Hansen, New York, NY).

Brightfield immunohistochemical staining

The same protocol used for immunofluorescence was performed to apply the primary and secondary antibodies. Slides were then incubated with a 3,3′-diaminobenzidine (DAB) chromogen (Vector Laboratories, San Mateo, CA) and then washed in running water for 5 minutes. They were then submerged in Gill Formula Hematoxylin (Vector Laboratories), and washed in running water. After rinsing, slides were dehydrated in a series of ethanol and xylene solutions. Once in xylene, slides were mounted with mounting media (Leica Biosystems, Danvers, MA) and coverslipped.

Slide imaging and quantification

Slides were digitally imaged using a Perkin Elmer Vectra Polaris slide scanner (Akoya Biosciences, Inc., Marlborough, MA) for both brightfield and darkfield microscopy at 40× and 20× magnification, respectively. Immunofluorescent slides were spectrally unmixed through Phenochart and InForm Image Analysis software (Akoya Biosciences) to remove autofluorescence. HALO (Indica Labs, Albuquerque, NM) and ImageScope software (Leica Biosystems) were used to process images and perform quantification analyses. Quantification of AT8 staining area and CD68 and Iba1 staining density was performed using previously described methods with ImageScope software (Leica Biosystems) (10, 51). Algorithms were designed to recognize Iba1+ microglia, CD68+ cells, and AT8+ neurofibrillary tangles in the cortical sulcal grey matter, anatomically defined as the bottom 1/3 of 2 connecting gyri and extending to the grey-white matter interface (10). We tuned each algorithm to recognize positive stained pixels on positively stained controls cases, then screened against negative control cases to ensure no background. AT8 results were expressed as positive-staining pixels/mm^2, while CD68 and Iba1+ staining results were expressed as positive-staining cells/mm^2. Quantification of ICAM1 staining at the sulcal depths, defined as the bottom third of adjacent gyri and including all of the connecting grey matter, and whole-section albumin staining was performed using the HALO algorithm Area Quantification v2.1.7 which calculated the area of positive staining and divided it by the total area analyzed to generate the percent positive area. Identification and quantification of fluorescent marker colocalization at the sulcal depths were performed using the HALO algorithm Area Quantification FL v2.1.5, which calculated the area of positive staining for multiple markers of interest divided by the total area analyzed to generate the percent area positive for marker colocalization (52–54).

Statistical methods

Statistical analyses were performed using SPSS version 26.0 (IBM Corp, Armonk, NY) and Prism v.8 (GraphPad Software, La Jolla, CA). ICAM1, VCAM1, and CRP DLF levels were nonnormally distributed, and were normalized by rank-based normalization in SPSS (v.26, IBM) (55). To assess for differences in demographic data, between group ANOVAs and chi-squared analyses were performed using SPSS. To compare the variation and means of each group's normalized immunoassay quantification data with all other groups, analysis of covariance (ANCOVA) was performed using age as a covariate in all models to adjust for its effects using SPSS. Results and data were graphed with GraphPad Prism. Associations between markers of vascular injury and factors of interest were determined by multiple linear regression models which used normalized data for the dependent variables. The relationship between ICAM1, VCAM1, and CRP DLF levels and RHI exposure duration was analyzed using multiple linear regression with age at death included as a covariate in the regression model in SPSS (v.26, IBM). The relationships between ICAM1, VCAM1, and CRP DLF levels and CD68 and Iba1 DLF staining density as well as tau pathology measures (including AT8 staining density and p-tau species) were tested separately using multiple linear regressions with age at death included as a covariate in the regression model in SPSS (v.26, IBM). The standardized β is reported for all linear regression results.

RESULTS

Demographic differences between experimental groups

Immunoassay group

All groups were exclusively male with one individual in the RHI No CTE group identifying as transgender. Experimental groups differed significantly in mean age, RHI exposure duration, and PMI. The High CTE group was found to have a lower frequency of soccer players compared to the other groups (p = 0.023) (Table 1).

Histology group

A subset of cases were selected for histological analysis (n = 57). All were male and had RHI exposure. Duration of RHI exposure and age were significantly increased in High CTE compared to No CTE group, but were not significantly different between No CTE and Low CTE groups. There was no difference in PMI between groups.

Markers of vascular injury are increased in CTE

To test the hypothesis that markers of vascular injury are increased within the frontal cortex of participants exposed to RHI and with CTE, levels of ICAM1, VCAM1, and CRP were quantitated in DLF tissue lysate and compared by ANCOVA, adjusting for age at death. We found significantly elevated levels of ICAM1 (p = 0.0002), VCAM1 (p = 0.0003), and CRP (p = 0.0427) in the high CTE group compared to the No RHI/No CTE control group (Fig. 1A–C). Compared to the RHI/No CTE group, there were significantly elevated levels of

CRP (p = 0.0487) in the low CTE group and significantly elevated levels of ICAM1 (p = 0.0049), VCAM1 (p < 0.0001), and CRP (p = 0.0214) in the high CTE group (Fig. 1A–C). VCAM1 (p = 0.0049) levels were significantly increased in high CTE compared to low CTE (Fig. 1B). Secondary analyses adjusting for postmortem interval (PMI) in addition to age produced similar results, with the exception of loss of statistical significance of the difference in CRP levels between the RHI No CTE and low CTE groups (p = 0.070). Eliminating the 12 cases with acute perimortem head trauma showed similar effect sizes and did not result in loss of significance for any results. We confirmed these findings by staining sections from the DLF for ICAM1 and quantitating positive staining. Histologically, the density of ICAM1 staining increased with CTE severity such that ICAM1 staining density at the sulcal depths was significantly increased in the High CTE group compared to the No CTE (p = 0.0001) and the Low CTE (p = 0.0151) groups (Figs. 2C and 3A). Two cases without RHI exposure stained for ICAM1 had immunoreactive pial microvasculature and leptomeninges, but did not show parenchymal staining in the grey matter.

RHI exposure is associated with increased markers of vascular damage

The association between of RHI exposure and markers of vascular injury was examined with immunohistochemistry and proteomics. Multiple linear regressions adjusting for age demonstrated that total years of contact sports participation were positively correlated with ICAM1 (ß = 0.168, p = 0.006) and CRP (ß = 0.196, p = 0.007) levels in all cases (Table 3).

Secondary analyses adjusting for PMI in addition to age showed similar effect sizes for ICAM1 and CRP levels. ICAM1 immunostaining was predominately associated with the vasculature, especially smaller caliber vessels in the cortical grey matter at the depths of the sulci in all RHI-exposed subjects (Fig. 2A, B). This was confirmed by multiplex IF colocalization quantification, which found that GLUT1, expressed by vascular endothelial cells, colocalized with ICAM1 consistently in all RHI-exposed cases (Fig. 3). Serum albumin was observed to have a diffuse, circular staining pattern immediately adjacent to the microvasculature in RHI-exposed subjects (Fig. 4A–C), but not in RHI-naïve subjects (Fig. 4D), and was not seen in those without any history of head impact exposure. Both the grey and white matter displayed albumin staining characteristic of microvascular leakage, with the cortical sulci and gyri affected equally. Some degree of albumin leakage was seen in almost all RHI-exposed cases but increased with CTE severity. Extravascular albumin staining was present in individuals with RHI both with and without evidence of acute head trauma, demonstrating that acute compromise of vascular integrity did not cause the staining pattern observed.

Markers of vascular injury are associated with microglial densities

In order to determine if the increased levels of vascular injury markers observed were associated with increased local levels of inflammatory cells, histological quantification of cells immunostained with the microglial markers Iba1 or CD68 was performed in the DLF. Microglia, the resident immune/macrophage cells of the CNS, interacts with ICAM1 and
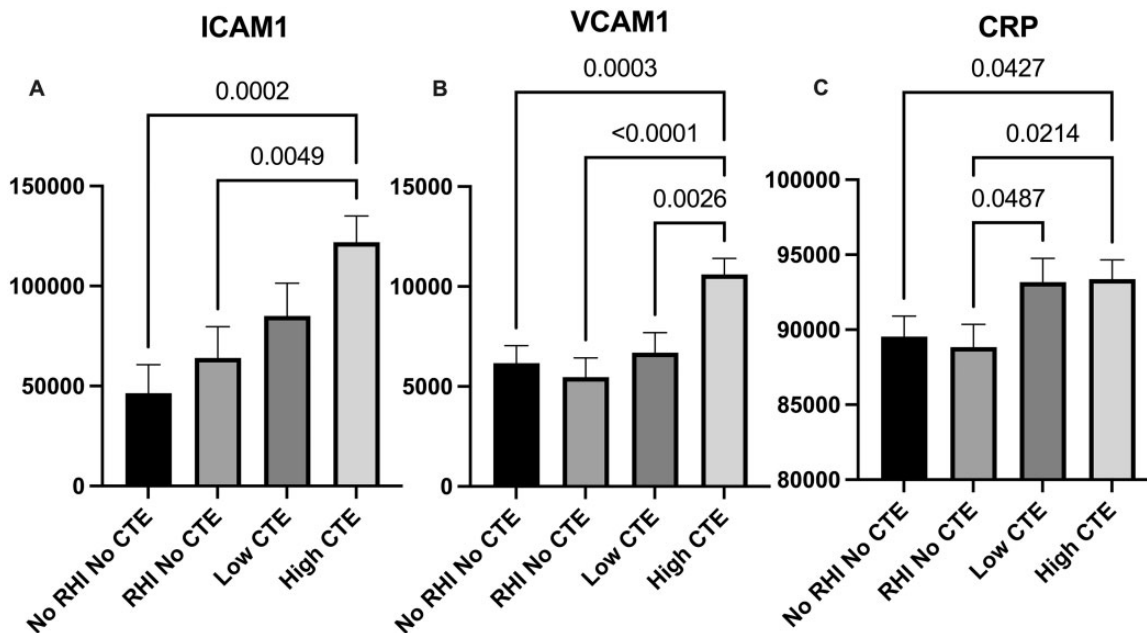
Figure 1. Quantification of vascular injury markers (**A**) ICAM1, (**B**) VCAM1, and (**C**) CRP levels in the dorsolateral frontal cortex. Immunoassay quantification of vascular injury markers in dorsolateral frontal (DLF) cortex. Data are grouped by CTE severity and RHI exposure (No RHI No CTE: n = 39, RHI No CTE: n = 36, Low CTE [McKee Stages I and II]: n = 31, High CTE [McKee Stages III and IV]: n = 50). Levels of all markers are expressed as pg/mL of tissue lysate. Differences in marker levels between groups are analyzed by ANCOVA adjusting for age with post hoc comparisons. All significant p values are shown on the graph. Results demonstrate that markers of vascular injury are increased in CTE compared to controls.
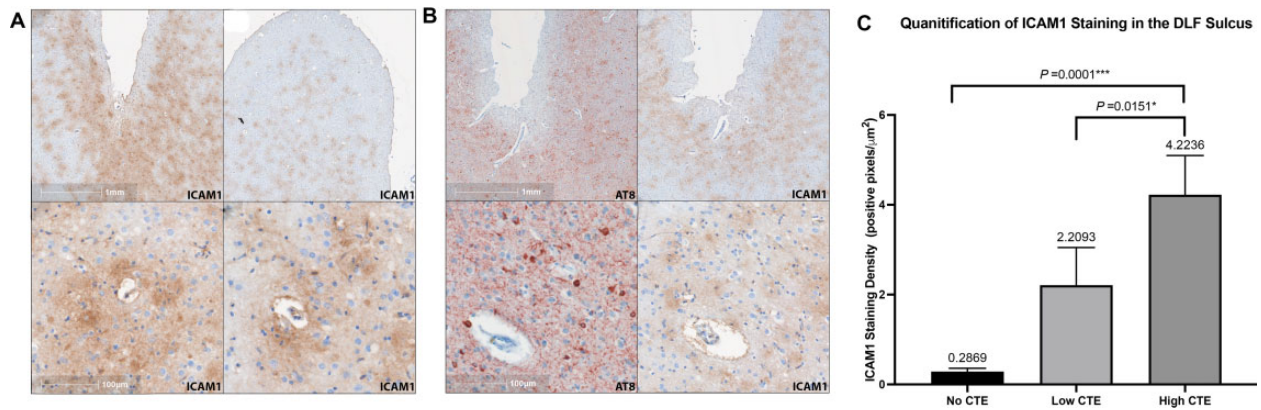
Figure 2. Immunohistochemical staining of ICAM1 in the dorsolateral frontal cortex sulcus and quantification of staining properties. ICAM1 IHC staining distribution shares similarities with CTE p-tau pathology in the DLF sulcus and is consistently associated with cortical microvasculature. **(A)** ICAM1 IHC of DLF sulcus in cases of High CTE. ICAM1 IHC staining intensity is greatest at the depths of the DLF sulci (top left) vs the crest of the gyrus (top right). ICAM1 IHC staining of the perivascular parenchyma under the depth of sulcus is demonstrated in the bottom panels. **(B)** IHC staining of the depth of the DLF sulcus in 2 separate cases (separated by rows) of High CTE. Left column: IHC staining for p-tau. Right column: IHC staining for ICAM1. **(C)** Histological quantification of ICAM1 staining area at the depths of the DLF sulcus. Results are displayed as positive staining density (positive pixels/total area analyzed). Data are grouped by CTE severity (No CTE n = 10, Low CTE n = 24, High CTE n = 23) with group means displayed above error bars. ANOVA found significant differences between groups (p = 0.0001) with significantly more ICAM1 staining in the High CTE group than the Low CTE group (p = 0.0151) and No CTE group (p = 0.0001).

VCAM1 via their ligand LFA1, with the LFA1-ICAM1/VCAM1 system facilitating microglial-mediated inflammation (30). We hypothesized that vascular injury markers would be associated with increased density of total (Iba1) and activated (CD68) microglia. Multiple linear regression demonstrated that the density of CD68 staining was, in fact, associated with increased levels of ICAM1 ($\beta = 0.291$, $p < 0.0001$), VCAM1 ($\beta = 0.381$, $p < 0.0001$), and CRP ($\beta = 0.326$, $p < 0.0001$) (Table 4). The density of Iba1 staining was positively correlated with VCAM1 levels ($\beta = 0.275$, $p = 0.0045$; Table 4). Secondary analyses adjusting for PMI in addition to age demonstrated that these associations remained intact and significant.

Vascular injury markers are associated with increased tau and amyloid pathology

Our recent study suggests that within the DLF, p-tau202 is a CTE-associated tau phosphorylation site, while p-tau396 is related to increased age and AD (9). Therefore, we tested the hypothesis that vascular injury markers would be associated with AT8 p-tau pathology burden within the sulcus as well as with increased levels of CTE-related p-tau epitopes. Multiple linear regressions adjusting for age showed that ICAM1 levels in the DLF were significantly associated with AT8 staining area ($\beta = 0.262$, $p < 0.0001$), p-tau202 ($\beta = 0.159$, $p = 0.017$), and p-tau396 ($\beta = 0.200$, $p = 0.002$). VCAM1 levels in the DLF were significantly negatively associated with p-tau181 ($\beta = -0.208$, $p = 0.017$) and positively with p-tau396 levels ($\beta = 0.239$, $p = 0.002$). CRP levels were significantly associated with AT8 staining area ($\beta = 0.183$, $p = 0.038$) and p-tau396 ($\beta = 0.171$, $p = 0.027$) (Table 5). No significant associations were found with p-tau231 levels. Levels of $A\beta_{1-40}$ were associated with ICAM1 ($\beta = 0.131$, $p = 0.046$) and CRP ($\beta = 0.163$, $p = 0.042$) DLF levels.

Colocalization and relationships between ICAM1, p-tau, and glia in CTE

The histological distribution of ICAM1 staining in CTE was patchy and occurred in the same regions with p-tau pathology (Fig. 2A, B). Both ICAM1 and AT8 staining was greatest at the sulcal depths and dramatically increased with CTE severity. Areas of higher p-tau burden, primarily perivascular parenchyma and sulcal depths, show increased staining of ICAM1 in CTE (Fig. 3A). In more severe CTE, ICAM1 also stained the cortical grey matter adjacent to the vasculature in cells with a stellate pattern that appear morphologically as astrocytes (Fig. 5). By using an IF multiplex panel that labeled GFAP, GLUT1, ICAM1, and p-tau (AT8), the spatial distribution and degree of colocalization of ICAM1 with glia and p-tau pathology at the sulcal depth could be quantitated for comparison between groups (Fig. 3). GLUT1, expressed by vascular endothelial cells, colocalized with ICAM1 in all groups without significant differences. In the High CTE group, ICAM1 colocalized with GFAP significantly more than in the Low CTE (p = 0.0031) and No CTE (p < 0.0001) groups (Fig. 3C). In High CTE, ICAM1 primarily colocalized with GFAP (34.4% total ICAM1) and GLUT1 (29.2% total ICAM1), and to a lesser extent AT8 (9.6% total ICAM1; some colocalized with multiple markers), while 49.6% of ICAM1 did not colocalize with any of these markers. ICAM1-GFAP colocalization occurred in a stellate pattern characteristic of astrocytes within the cortical grey matter and tended to be adjacent to p-tau lesions (Fig. 3B). There was significantly more ICAM1 colocalized with AT8 in the High CTE group when compared to Low CTE (p = 0.0002) and No CTE (p < 0.0001) groups at the depths of the DLF sulcus (Fig. 3C). ICAM1, GFAP, and AT8 were found to colocalize together significantly more in the High CTE than in the Low CTE (p = 0.0002) and No CTE (p < 0.0001) groups (Fig. 3C).
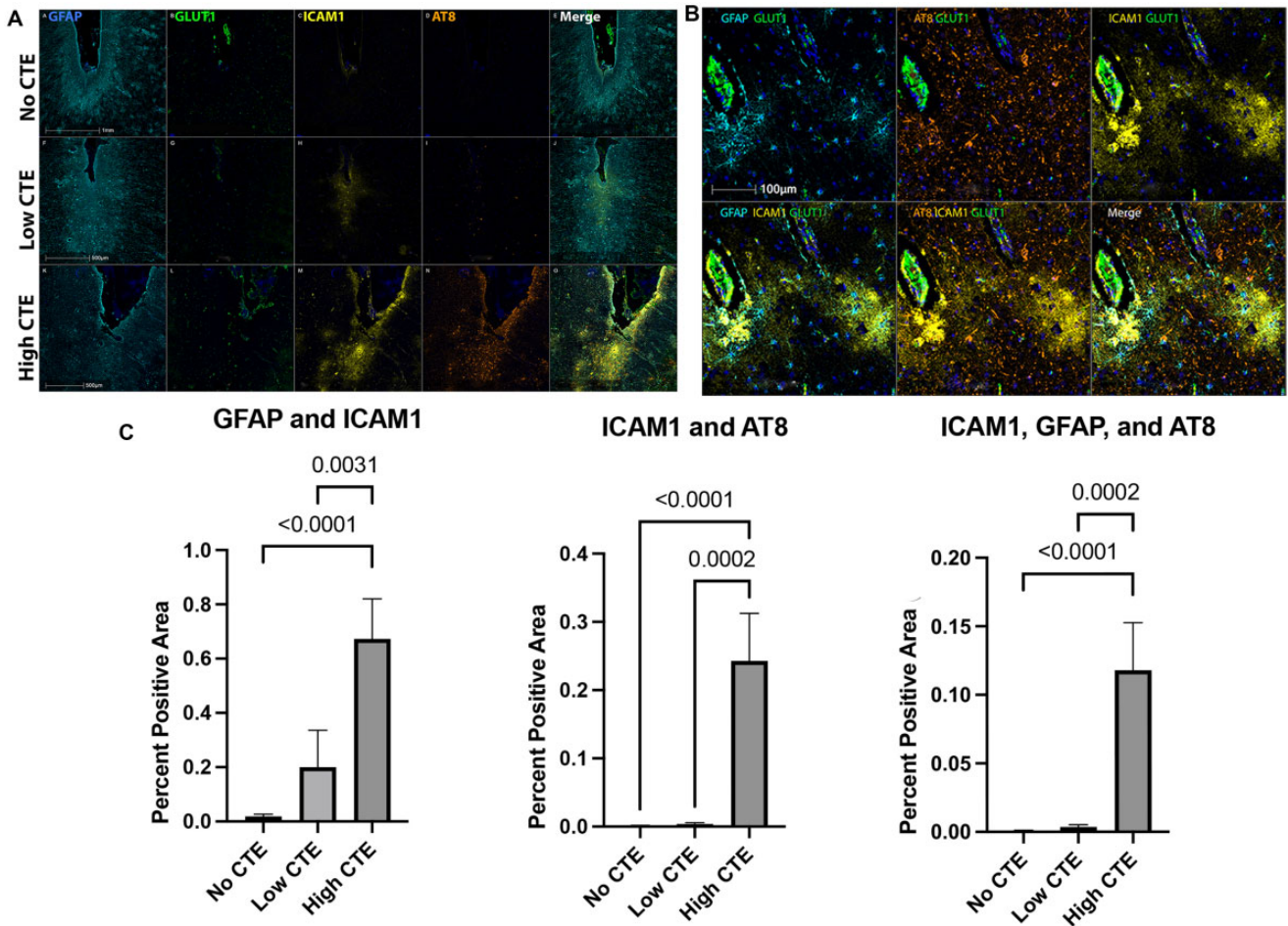
Figure 3. Multiplex immunofluorescence showing colocalization of ICAM1 with p-tau and astrocytic markers in higher severity CTE. Dorsolateral frontal cortex sections stained for an mIF panel targeting ICAM1, AT8, and GFAP demonstrate colocalization of ICAM1 with both astrocytes and p-tau pathology as CTE severity increases. **(A)** Immunofluorescent multiplex staining of DLF depth of sulcus sections from 3 cases: No CTE (top row), Low CTE (middle row), and High CTE (bottom row). Markers targeted are GFAP (teal), GLUT1 (green), ICAM1 (yellow), p-tau (AT8; orange), and DAPI (blue). Scale bar: 100 μm (the same for all panels). **(B)** Immunofluorescent multiplex staining illustrating ICAM1, GFAP, and p-tau colocalization in High CTE. Single markers: GFAP: teal, AT8: orange, ICAM1: yellow, GLUT1 (green), and DAPI (blue). Scale bar is the same for all panels. **(C)** Histological quantification of florescent marker colocalization. Results presented as percent positive area (area positive for markers of interest/total area analyzed) and grouped by CTE severity (No CTE n = 10, Low CTE n = 24, High CTE n = 23). Results analyzed by Kruskal-Wallis one-way ANOVA with Dunn multiple comparisons. GFAP-ICAM1 group means were significantly different ($p < 0.0001$), with significantly more GFAP-ICAM1 colocalization in High CTE compared to Low CTE ($p = 0.0031$) and No CTE ($p < 0.0001$). ICAM1-AT8 group means were significantly different ($p < 0.0001$), with significantly more AT8-ICAM1 colocalization in High CTE compared to Low CTE ($p = 0.0002$) and No CTE ($p < 0.0001$). ICAM1-AT8-GFAP group means were significantly different ($p < 0.0001$), with significantly more AT8-GFAP-ICAM1 colocalization in High CTE compared to Low CTE ($p = 0.0002$) and No CTE ($p < 0.0001$).

DISCUSSION

Levels of the vascular injury-associated markers ICAM1, VCAM1, and CRP were increased in in CTE compared to those without disease and increased with CTE severity. Increased duration of RHI exposure was significantly associated with increased ICAM1 and CRP. Cellular adhesion molecules are known to attract inflammatory cells (56), and we found that ICAM1, VCAM1, and CRP levels were associated with increased CD68+ cell density (Table 4). All RHI-exposed cases demonstrated extravascular albumin staining in both the gray and white matter of the DLF that was not observed in RHI-naïve cases, suggesting that vascular compromise is an early and chronic phenomenon after RHI exposure. Antemortem white matter hyperintensities on MRI have been associated with years of football play, arteriolosclerosis, and white matter rarefaction (57). These hyperintensities may also reflex vascular leakage although current imaging modalities likely do not allow for resolution of very small serum leakage (57). Histological analysis demonstrated that p-tau and ICAM1 colocalized at the depth of the sulcus. Thus, in CTE, the DLF sulcus, a region with known susceptibility to RHI (15, 18), is a focus for vascular damage, microglial activation,

Table 3. Vascular injury markers are associated with increased RHI duration

	ICAM1 (pg/mL)		VCAM1 (pg/mL)		CRP (pg/mL)	
	ß	p value	ß	p value	ß	p value
RHI exposure, years	**0.168**	**0.006**	0.074	0.308	**0.196**	**0.007**

Multiple linear regressions adjusting for age at death; n = 156.
RHI: repetitive head impacts.
All significant results (p < 0.05) are displayed in bold font.
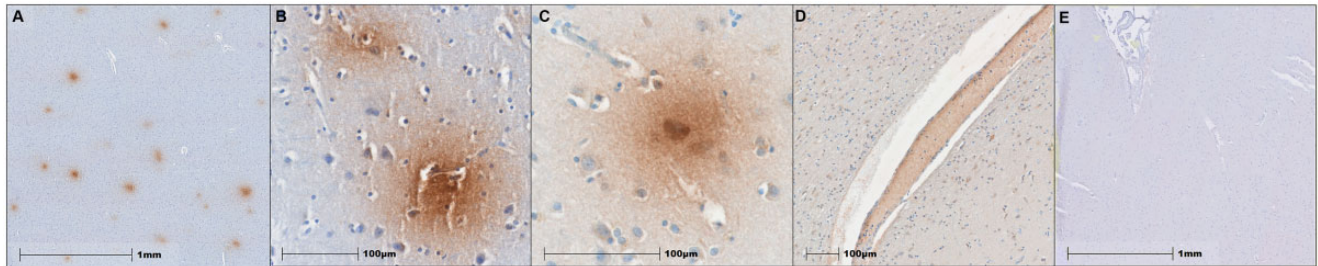
Figure 4. Serum albumin IHC demonstrates vascular leakage in CTE and RHI-exposed cases, but not in RHI-naïve cases. Albumin IHC staining within the dorsolateral frontal sulcus from 3 RHI-exposed cases (**A–D**) and 1 RHI-naïve case (**E**). Positive staining surrounding the microvasculature indicates leakage of serum proteins into parenchyma, while intravascular staining confirms labeling of serum albumin (**D**).

Table 4. Vascular injury marker levels are associated with CD68 and Iba1 cellular density

	ICAM1 (pg/mL)		VCAM1 (pg/mL)		CRP (pg/mL)	
	ß	p value	ß	p value	ß	p value
CD68 density in DLF sulcus (positive-staining cells/mm^2)	**0.291**	**<0.0001**	**0.381**	**<0.0001**	**0.326**	**<0.0001**
Iba1 density in DLF sulcus (positive-staining cells/mm^2)	0.102	0.198	**0.275**	**0.0045**	0.169	0.088

Multiple linear regressions adjusting for age; n = 156.
All significant results (p < 0.05) are displayed in bold font.

and p-tau pathology. In fact, vascular injury markers were associated with increased p-tau pathology and may be involved in the pathogenesis of CTE.

Increased vascular injury markers and neurovascular-mediated inflammation associated with RHI-exposure and CTE

Levels of ICAM1, VCAM1, and CRP, markers of vascular injury, were associated with RHI exposure and CTE status. ICAM1 and CRP were found to be significantly positively associated with the duration of RHI exposure, suggesting that vascular damage persists and its severity is related to years of contact sports play. Extravascular albumin staining was present in RHI-exposed individuals without acute head trauma, demonstrating that acute compromise of vascular integrity was not the cause of the multifocal perivascular staining observed (Fig. 4).

Although endothelial cells have been shown to be a source of ICAM1, VCAM1, and CRP (33, 58), our results demonstrate that ICAM1 is associated with both vascular endothelial cells and astrocytes following RHI. While the majority of ICAM1 appeared to be soluble in the extracellular matrix, ICAM1 was found to colocalize with the endothelial cell marker GLUT1 in all cases, as well as with the astrocyte marker GFAP in cases of CTE to a significantly greater degree compared to controls. Therefore, a longer period of RHI may lead to persistent endothelial cell injury and chronic production of ICAM1, VCAM1, and CRP. Additionally, tissue damage may lead to greater astrocytic production of ICAM1. Future studies examining cell specific gene expression such as in situ hybridization may help further identify the source of increased ICAM1 following RHI and in CTE. In fact, a recent report by Chancellor et al (59) found unique populations of astrocytes with upregulated neuroinflammation-associated transcripts and evidence of altered iron processing by oligodendrocytes in white matter in CTE, supporting the hypothesis that vascular and glial elements synergistically promote and respond to neuroinflammation.

Vascular injury may promote tissue damage

Proteins associated with vascular injury may play important roles in mediating chronic tissue damage following RHI. Increased vascular leakage in CTE may have several important implications. First, inadequate delivery of nutrients to and removal of waste from the neuropil acts to slowly damage neurons and glial cells. Hypoxia due to poor blood flow is an

Table 5. Associations between vascular injury marker levels and tau pathology measures

DLF levels (pg/mL)	AT8 staining area in DLF sulcus (positive staining pixels/total pixels)		pTau-181 (units/mL)		pTau-202 (µg/g)		pTau-231 (µg/g)		pTau396 (µg/g)	
	ß	p value	ß	p value	ß	p value	ß	p value	ß	p value
ICAM1	**0.262**	**<0.0001**	−0.072	0.333	**0.159**	**0.017**	0.028	0.655	**0.200**	**0.002**
VCAM1	0.158	0.071	**−0.208**	**0.017**	0.098	0.220	0.069	0.343	**0.239**	**0.002**
CRP	**0.183**	**0.038**	−0.037	0.671	0.050	0.521	−0.108	0.142	**0.171**	**0.027**

Multiple linear regressions adjusted for age; n = 156.
All significant results (p < 0.05) are displayed in bold font.
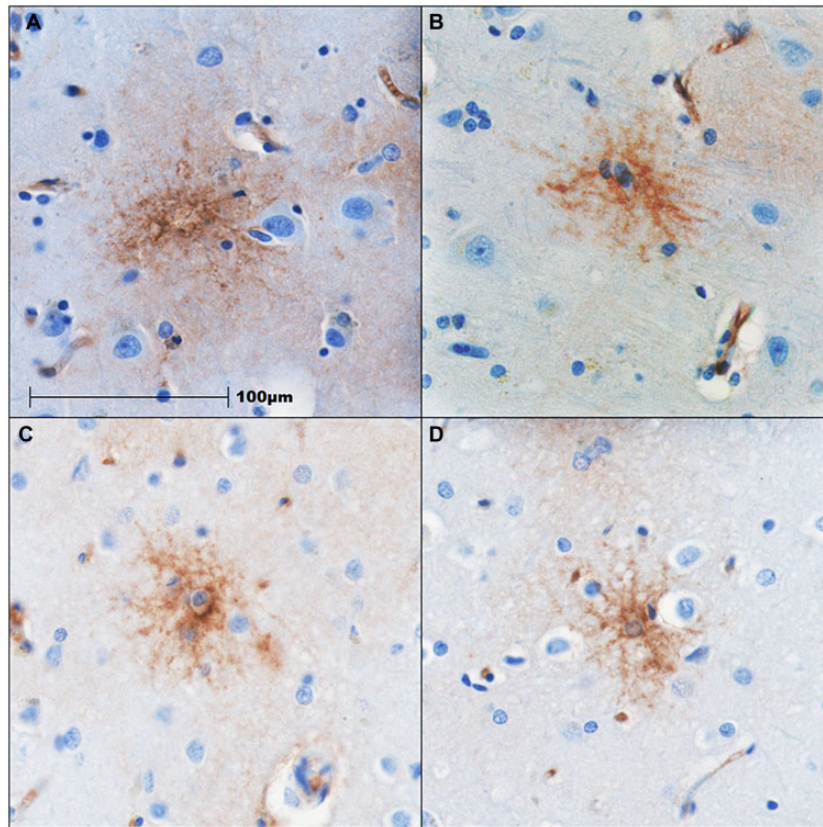
Figure 5. Stellate morphology of ICAM1 IHC staining in high CTE. IHC staining for ICAM1 in the cortical grey matter at the depth of the DLF sulcus. Panels above show positive staining in stellate pattern in cells morphologically resembling astrocytes from 4 cases of CTE (Stage III [**A, B**] and Stage IV [**C, D**]). Scale bar: 100 µm (the same for all panels).

important trigger of inflammation and may play a role in how these processes are propagated in CTE. Second, serum proteins such as albumin and fibrinogen/fibrin can activate astrocytes and microglia (22). Fibrinogen/fibrin is a ligand for ICAM1, which may increase its expression and activity, and has been reported to promote neuronal degeneration in AD (60). Serum albumin binding to astrocytes stimulates their production of matrix metalloproteases as well as acting to increase vessel permeability along with fibrinogen (22, 23, 61). Finally, chronic vascular incompetence leading to low level tissue hypoxia has been shown to increase production of angiogenic proteins such as vascular endothelial growth factor, as well as newly implicated molecules such as monomeric CRP, in order to promote neoangiogenesis and increase collateral circulation (40, 62–64). All of these factors can increase BBB permeability and may promote tissue damage if chronically elevated.

Recruitment of activated microglia and associations with tau pathology

ICAM1, VCAM1, and CRP are active in multiple pathways, many of which promote inflammation. Chronic elevation of these proteins may lead to tissue injury and recognition of damage-associated molecular patterns (DAMPs) by the innate immune system (65). ICAM1 and VCAM1 act as ligands for microglia as well as modulate the expression of chemotactic

factors (66). Cherry et al (67) previously reported increased local levels of microglia chemoattractant monocyte chemoattractant protein 1 (CCL2) in CTE that are positively associated with regional DLF p-tau burden. We found that in CTE, ICAM1, VCAM1, and CRP DLF levels were positively associated with the lysosomal marker CD68, which stains activated microglia and macrophages, and VCAM1 was further positively associated with Iba1, a marker of total microglia and macrophages. Cherry et al (10) demonstrated increased microglial inflammation after RHI and a progressive increase in microgliosis with increasing CTE p-tau pathology, suggesting that inflammation drives p-tau pathology and increased p-tau pathology promotes persistent high levels of inflammation. Cell culture and animal models support this hypothesis and have found that neuroinflammation favors the formation and accumulation of p-tau (64, 68). Therefore, ICAM1-associated microgliosis may be a possible mechanism by which ICAM1 expression leads to increased tau pathology in CTE.

Indeed, we found ICAM1, VCAM1, and CRP DLF levels to be significantly associated with proteomic and histological quantification of p-tau. The pattern of ICAM1 immunostaining closely mirrored that of p-tau pathology in CTE in that it was most concentrated at the sulcal depths and around blood vessels and was often in the same location as p-tau lesions. Furthermore, proteomics and multiple linear regression showed that both ICAM1 and CRP were associated with increased AT8-positive p-tau pathology and p-tau396, while ICAM1 was additionally associated with p-tau202. Tau phosphorylated at Serine202 has recently been associated with RHI and may represent a phosphorylation site more sensitive to RHI and CTE. Tau phosphorylated at Serine396 is also elevated in CTE, with significantly more in high severity, but was associated with age and β-amyloid levels in our previous study (9).

Limitations and future directions

There are several limitations to this study. Assessment of vascular injury may be hindered by postmortem change. However, adjusting for PMI did not substantially change our results. Select markers of vascular injury were examined, but these may be involved in other processes as well and future studies should examine additional measures of vascular injury. Transcriptomic methods such as in situ hybridization and single nuclear RNAseq could be used to determine the cellular source of these proteins. As vascular injury is often association with neoangiogenesis and blood vessel morphology is altered in CTE, future studies should examine associations between RHI and ICAM1 with angiogenesis and vessel morphology in CTE. Markers of vascular injury, including ICAM1 and CRP, may be potential diagnostic biomarkers and therapeutic targets for CTE, and future work might also examine levels in cerebrospinal fluid and blood as has been done with acute TBI and AD (37, 69–73).

Conclusion

Overall, we find increased markers of vascular damage and intraparenchymal serum protein leakage associated with RHI-exposure and CTE that persists decades after a period of RHI.

These findings highlight vascular injury as a persistent and potentially early change following RHI and CTE and future studies should continue to examine markers of vascular injury and neuroinflammation as potential targets for the diagnosis, treatment, and prevention of brain injury and CTE.

CONFLICT OF INTEREST

The authors have no duality or conflicts of interest to declare.

SUPPLEMENTARY DATA

Supplementary Data can be found at academic.oup.com/jnen.

DATA AVAILABILITY

The data that support the findings of this study are available from the corresponding author upon reasonable request.

REFERENCES

1. McKee AC, Stein TD, Nowinski CJ, et al. The spectrum of disease in chronic traumatic encephalopathy. Brain 2013;136:43–64
2. Alosco ML, Cherry JD, Huber BR, et al. Characterizing tau deposition in chronic traumatic encephalopathy (CTE): Utility of the McKee CTE staging scheme. Acta Neuropathol 2020;140:495–512
3. McKee AC, Cairns NJ, Dickson DW, et al.; TBI/CTE Group. The first NINDS/NIBIB consensus meeting to define neuropathological criteria for the diagnosis of chronic traumatic encephalopathy. Acta Neuropathol 2016;131:75–86
4. Bieniek KF, Cairns NJ, Crary JF, et al. The Second NINDS/NIBIB Consensus Meeting to define neuropathological criteria for the diagnosis of chronic traumatic encephalopathy. J Neuropathol Exp Neurol 2021;80:210–9

5. Daneshvar DH, Nowinski CJ, McKee AC, Cantu RC. The epidemiology of sport-related concussion. Clin Sports Med 2011;30:1–17

6. Mez J, Daneshvar DH, Abdolmohammadi B, et al. Duration of American football play and chronic traumatic encephalopathy. Ann Neurol 2020;87:116–31

7. McKee AC, Cantu RC, Nowinski CJ, et al. Chronic traumatic encephalopathy in athletes: Progressive tauopathy after repetitive head injury. J Neuropathol Exp Neurol 2009;68:709–35

8. McKee AC, Stein TD, Kiernan PT, et al. The neuropathology of chronic traumatic encephalopathy. Brain Pathol 2015;25:350–64

9. Stathas S, Alvarez VE, Xia W, et al. Tau phosphorylation sites serine202 and serine396 are differently altered in chronic traumatic encephalopathy and Alzheimer's disease. Alzheimers Dement 2022; 18:1511–22

10. Cherry JD, Tripodis Y, Alvarez VE, et al. Microglial neuroinflammation contributes to tau accumulation in chronic traumatic encephalopathy. Acta Neuropathol Commun 2016;4:112

11. Maphis N, Xu G, Kokiko-Cochran ON, et al. Reactive microglia drive tau pathology and contribute to the spreading of pathological tau in the brain. Brain 2015;138:1738–55

12. McKee AC, Daneshvar DH, Alvarez VE, Stein TD. The neuropathology of sport. Acta Neuropathol 2014;127:29–51

13. Veksler R, Vazana U, Serlin Y, et al. Slow blood-to-brain transport underlies enduring barrier dysfunction in American football players. Brain 2020;143:1826–42

14. Doherty CP, O'Keefe E, Wallace E, et al. Blood-brain barrier dysfunction as a hallmark pathology in chronic traumatic encephalopathy. J Neuropathol Exp Neurol 2016;75:656–62

15. Cloots RJH, Gervaise HMT, van Dommelen JAW, et al. Biomechanics of traumatic brain injury: Influences of the morphologic heterogeneities of the cerebral cortex. Ann Biomed Eng 2008;36: 1203–15

16. O'Keeffe E, Kelly E, Liu Y, et al. Dynamic blood–brain barrier regulation in mild traumatic brain injury. J Neurotrauma 2020;37: 347–56

17. Bandak FA, Ling G, Bandak A. Injury biomechanics, neuropathology, and simplified physics of explosive blast and impact mild traumatic brain injury. In: Grafman J, Salazar AM, eds. Handbook of Clinical Neurology. Amsterdam, Netherlands: Elsevier BV; 2015:89–104

18. Ghajari M, Hellyer PJ, Sharp DJ. Computational modelling of traumatic brain injury predicts the location of chronic traumatic encephalopathy pathology. Brain 2017;140:333–43

19. Silver JM, McAllister TW, Yudofsky SC. Textbook of Traumatic Brain Injury. 1st ed. Washington, DC: American Psychiatric Pub; 2005:771

20. Browne KD, Chen XH, Meaney DF, et al. Mild traumatic brain injury and diffuse axonal injury in swine. J Neurotrauma 2011;28: 1747–55

21. Mckee AC, Daneshvar DH, Chapter 4: The neuropathology of traumatic brain injury. In: Grafman J, Salazar AM, eds. Handbook of Clinical Neurology. Amsterdam: Elsevier; 2015:45–66

22. Ralay Ranaivo H, Wainwright MS. Albumin activates astrocytes and microglia through mitogen-activated protein kinase pathways. Brain Res 2010;1313:222–31

23. Ranaivo HR, Hodge JN, Choi N, et al. Albumin induces upregulation of matrix metalloproteinase-9 in astrocytes via MAPK and reactive oxygen species-dependent pathways. J Neuroinflammation 2012;9:68

24. Petersen MA, Ryu JK, Akassoglou K. Fibrinogen in neurological diseases: Mechanisms, imaging and therapeutics. Nat Rev Neurosci 2018;19:283–301

25. Muradashvili N, Tyagi SC, Lominadze D. Localization of fibrinogen in the vasculo-astrocyte interface after cortical contusion injury in mice. Brain Sci 2017;7:77

26. Hay JR, Johnson VE, Young AMH, et al. Blood-brain barrier disruption is an early event that may persist for many years after traumatic brain injury in humans. J Neuropathol Exp Neurol 2015;74: 1147–57

27. Danton GH, Dietrich WD. Inflammatory mechanisms after ischemia and stroke. J Neuropathol Exp Neurol 2003;62:127–36

28. Arand M, Melzner H, Kinzl L, et al. Early inflammatory mediator response following isolated traumatic brain injury and other major trauma in humans. Langenbecks Arch Surg 2001;386:241–8

29. Al-Baradie RS, Pu S, Liu D, et al. Monomeric C-reactive protein localized in the cerebral tissue of damaged vascular brain regions is associated with neuro-inflammation and neurodegeneration—An immunohistochemical study. Front Immunol 2021;12:674

30. Greenwood J, Etienne-Manneville S, Adamson P, et al. Lymphocyte migration into the central nervous system: Implication of ICAM-1 signalling at the blood–brain barrier. Vascul Pharmacol 2002;38:315–22

31. Diamond MS, Staunton DE, de Fougerolles AR, et al. ICAM-1 (CD54): A counter-receptor for Mac-1 (CD11b/CD18). J Cell Biol 1990;111:3129–39

32. Berlin C, Bargatze RF, Campbell JJ, et al. α4 integrins mediate lymphocyte attachment and rolling under physiologic flow. Cell 1995; 80:413–22

33. Dean DC, Iademarco MF, Rosen GD, et al. The integrin $\alpha4\beta1$ and its counter receptor VCAM-1 in development and immune function. Am Rev Respir Dis 1993;148:S43–6

34. McKeating EG, Andrews PJ, Mascia L. The relationship of soluble adhesion molecule concentrations in systemic and jugular venous serum to injury severity and outcome after traumatic brain injury. Anesth Analg 1998;86:759–65

35. Shahrokhi N, Soltani Z, Khaksari M, et al. The serum changes of neuron-specific enolase and intercellular adhesion molecule-1 in patients with diffuse axonal injury following progesterone administration: A randomized clinical trial. Arch Trauma Res 2016;5: e37005

36. McKeating EG, Andrews PJD, Mascia L. Leukocyte adhesion molecule profiles and outcome after traumatic brain injury. In: Marmarou A, Bullock R, Avezaat C, Baethmann A, Becker D, Brock M, Hoff J, Nagai H, Reulen H-J, Teasdale G, eds. Intracranial Pressure and Neuromonitoring in Brain Injury. Vienna: Springer; 1998:200–2

37. Pleines UE, Stover JF, Kossmann T, et al. Soluble ICAM-1 in CSF coincides with the extent of cerebral damage in patients with severe traumatic brain injury. J Neurotrauma 1998;15:399–409

38. Akiyama H, Kawamata T, Yamada T, et al. Expression of intercellular adhesion molecule (ICAM)-1 by a subset of astrocytes in Alzheimer disease and some other degenerative neurological disorders. Acta Neuropathol 1993;85:628–34

39. Yasojima K, Schwab C, McGeer EG, McGeer PL. Human neurons generate C-reactive protein and amyloid P: Upregulation in Alzheimer's disease. Brain Res 2000;887:80–9

40. McFadyen JD, Zeller J, Potempa LA, et al. C-reactive protein and its structural isoforms: An evolutionary conserved marker and central player in inflammatory diseases and beyond. In: Hoeger U, Harris JR, eds. Vertebrate and Invertebrate Respiratory Proteins, Lipoproteins and Other Body Fluid Proteins. Switzerland: Springer International Publishing; 2020:499–520

41. Braig D, Nero TL, Koch HG, et al. Transitional changes in the CRP structure lead to the exposure of proinflammatory binding sites. Nat Commun 2017;8:1–19

42. McFadyen JD, Kiefer J, Braig D, et al. Dissociation of C-reactive protein localizes and amplifies inflammation: Evidence for a direct biological role of C-reactive protein and its conformational changes. Front Immunol 2018;9:1351

43. Newell KL, Hyman BT, Growdon JH, et al. Application of the National Institute on Aging (NIA)-Reagan Institute criteria for the neuropathological diagnosis of Alzheimer disease. J Neuropathol Exp Neurol 1999;58:1147–55

44. Hyman BT, Phelps CH, Beach TG, et al. National Institute on Aging–Alzheimer's Association guidelines for the neuropathologic

assessment of Alzheimer's disease. Alzheimers Dement 2012;8: 1–13

45. Mez J, Solomon TM, Daneshvar DH, et al. Assessing clinicopathological correlation in chronic traumatic encephalopathy: Rationale and methods for the UNITE study. Alzheimers Res Ther 2015; 7:62

46. Vonsattel JPG, del Amaya MP, Keller CE. Twenty-first century brain banking. Processing brains for research: The Columbia University methods. Acta Neuropathol 2008;115:509–32

47. Friedman MJ, Huber BR, Brady CB, et al.; Traumatic Stress Brain Research Group. VA's National PTSD Brain Bank: A national resource for research. Curr Psychiatry Rep 2017;19:73

48. Stein TD, Montenigro PH, Alvarez VE, et al. Beta-amyloid deposition in chronic traumatic encephalopathy. Acta Neuropathol 2015; 130:21–34

49. Friedberg JS, Aytan N, Cherry JD, et al. Associations between brain inflammatory profiles and human neuropathology are altered based on apolipoprotein E ε4 genotype. Sci Rep 2020;10:2924

50. Chen M, Song H, Cui J, et al. Proteomic profiling of mouse brains exposed to blast-induced mild traumatic brain injury reveals changes in axonal proteins and phosphorylated tau. J Alzheimers Dis 2018;66:751–73

51. Bachstetter AD, Van Eldik LJ, Schmitt FA, et al. Disease-related microglia heterogeneity in the hippocampus of Alzheimer's disease, dementia with Lewy bodies, and hippocampal sclerosis of aging. Acta Neuropathol Commun 2015;3:1–16

52. André P, Denis C, Soulas C, et al. Anti-NKG2A mAb is a checkpoint inhibitor that promotes anti-tumor immunity by unleashing both T and NK cells. Cell 2018;175:1731–43.e13

53. Greenberg A, Huber BR, Liu DX, et al. Quantification of viral and host biomarkers in the liver of rhesus macaques: A longitudinal study of Zaire Ebolavirus Strain Kikwit (EBOV/Kik). Am J Pathol 2020;190:1449–60

54. Cherry JD, Kim SH, Stein TD, et al. Evolution of neuronal and glial tau isoforms in chronic traumatic encephalopathy. Brain Pathol 2020;30:913–25

55. Templeton GF. A two-step approach for transforming continuous variables to normal: Implications and recommendations for IS research. Commun Assoc Inf Syst 2011;28:4

56. Kim I, Moon SO, Kim SH, et al. Vascular endothelial growth factor expression of intercellular adhesion molecule 1 (ICAM-1), vascular cell adhesion molecule 1 (VCAM-1), and E-selectin through nuclear factor-κB activation in endothelial cells. J Biol Chem 2001; 276:7614–20

57. Uretsky M, Bouix S, Killiany RJ, et al. Association between antemortem FLAIR white matter hyperintensities and neuropathology in brain donors exposed to repetitive head impacts. Neurology 2022;98:e27–39

58. Dietrich JB. The adhesion molecule ICAM-1 and its regulation in relation with the blood–brain barrier. J Neuroimmunol 2002;128: 58–68

59. Chancellor KB, Chancellor SE, Duke-Cohan JE, et al. Altered oligodendroglia and astroglia in chronic traumatic encephalopathy. Acta Neuropathol 2021;142:295–321

60. Cortes-Canteli M, Mattei L, Richards AT, et al. Fibrin deposited in the Alzheimer's disease brain promotes neuronal degeneration. Neurobiol Aging 2015;36:608–17

61. Sumagin R, Kuebel JM, Sarelius IH. Leukocyte rolling and adhesion both contribute to regulation of microvascular permeability to albumin via ligation of ICAM-1. Am J Physiol Cell Physiol 2011;301:C804–13

62. Holmes DI, Zachary I. The vascular endothelial growth factor (VEGF) family: Angiogenic factors in health and disease. Genome Biol 2005;6:209

63. Hess DC, Zhao W, Carroll J, et al. Increased expression of ICAM-1 during reoxygenation in brain endothelial cells. Stroke 1994;25: 1463–7; discussion 1468

64. Snyder B, Shell B, Cunningham JT, et al. Chronic intermittent hypoxia induces oxidative stress and inflammation in brain regions associated with early-stage neurodegeneration. Physiol Rep 2017;5: e13258

65. Piccinini AM, Midwood KS. DAMPening inflammation by modulating TLR signalling. Mediators Inflamm 2010;2010:672395

66. Constantin G. Chemokine signaling and integrin activation in lymphocyte migration into the inflamed brain. J Neuroimmunol 2008; 198:20–6

67. Cherry JD, Meng G, Daley S, et al. CCL2 is associated with microglia and macrophage recruitment in chronic traumatic encephalopathy. J Neuroinflammation 2020;17:1–12

68. Lee DC, Rizer J, Selenica MLB, et al. LPS-induced inflammation exacerbates phospho-tau pathology in rTg4510 mice. J Neuroinflammation 2010;7:56–16

69. Sharief MK, Noori MA, Ciardi M, et al. Increased levels of circulating ICAM-1 in serum and cerebrospinal fluid of patients with active multiple sclerosis. Correlation with TNF-α and blood-brain barrier damage. J Neuroimmunol 1993;43:15–21

70. Zuliani G, Cavalieri M, Galvani M, et al. Markers of endothelial dysfunction in older subjects with late onset Alzheimer's disease or vascular dementia. J Neurol Sci 2008;272:164–70

71. Janelidze S, Mattsson N, Stomrud E, et al. CSF biomarkers of neuroinflammation and cerebrovascular dysfunction in early Alzheimer disease. Neurology 2018;91:e867–77

72. Ewers M, Mielke MM, Hampel H. Blood-based biomarkers of microvascular pathology in Alzheimer's disease. Exp Gerontol 2010;45:75–9

73. Fernandes A, Tábuas-Pereira M, Duro D, et al. C-reactive protein as a predictor of mild cognitive impairment conversion into Alzheimer's disease dementia. Exp Gerontol 2020;138:111004